Critical-Mode-Based Soft-Switching Modulation for Three-Phase Rectifiers

Zhengrong Huang[1], Zhengyang Liu[1], Fred C. Lee[1], Qiang Li[1], Furong Xiao[1,2]
[1]Center for Power Electronics Systems
The Bradley Department of Electrical and Computer Engineering
Virginia Polytechnic Institute and State University, Blacksburg, VA, USA
[2]School of Automation, Beijing Institute of Technology, Beijing, China
Email: zrhuang7@vt.edu

***Abstract*—In this paper, a novel critical-conduction-mode (CRM)-based soft-switching modulation is applied into three-phase rectifier application. With this modulation, zero-voltage-switching (ZVS) soft switching turn-on is achieved and the efficiency of the rectifier is improved, especially for high frequency operation with SiC MOSFETs, whose turn-on energy is large while the turn-off energy is negligible. In three-phase electric vehicle (EV) charging station applications, by operating at above 300 kHz switching frequency, system power density is estimated to be at least five times higher than commercial products, while efficiency is estimated to be 98% ~ 99% with soft switching. Non-zero-voltage-switching (Non-ZVS) issue and instability issue are solved and good performance of the proposed modulation under rectifier mode operation is verified with simulation analysis. A 25kW SiC-based three-phase bi-directional AC/DC converter prototype is built with 80W/in^3 power density. All the control functions are digitally implemented and experimentally verified on this prototype, and 99% peak efficiency is achieved for both inverter mode and rectifier mode operations at above 300 kHz high switching frequency.**

Keywords—critical conduction mode (CRM); soft switching; three-phase rectifier; silicon carbide MOSFET; digital control

I. INTRODUCTION

Three-phase rectifiers are widely used in the AC/DC stage of electric vehicle (EV) charging station applications. From the survey results of existing EV charging stations, the efficiency of the AC/DC stage is usually 96% ~ 97%, and the power density is usually up to 10 ~ 15 W/in^3 [1-5]. However, there is limited room for improvement in both the efficiency and the power density, because Si IGBT semiconductor devices are usually used in these systems and the operating switching frequency is around 20 kHz, which is already close to the frequency limit of Si IGBT devices.

With SiC MOSFET semiconductor devices, switching frequency can be pushed higher and good performance is still achievable, because SiC MOSFET devices have better figure-of-merit (FOM), which means smaller device loss compared with Si IGBT devices under the same operating condition. With more than ten times higher switching frequency, size reduction of passive components, such as inductors, harmonic and EMI filters, is achieved [6-7], and at least five times power density improvement compared with the existing EV charging station systems is expected.

For SiC MOSFET devices, the turn-on energy is relatively large while the turn-off energy is negligible [8-10]. In order to achieve high efficiency at several hundred of kHz high switching frequency operation, critical conduction mode (CRM) becomes the preferred operation mode for SiC MOSFET devices. This is because with CRM operation, zero-voltage-switching (ZVS) soft switching turn-on is achievable, which eliminates the relatively high turn-on loss, while only small price is paid on the turn-off loss and conduction loss due to the increase of inductor current ripple. With soft switching, the switching loss of the devices becomes small and high efficiency is achieved, even when the system is operating at hundreds of kHz high switching frequency.

Therefore, soft switching is the key to achieve high efficiency at high frequency operation; CRM operation is the simplest way to achieve soft switching without adding physical complexity to the system, and ZVS turn-on is beneficial to SiC MOSFET devices, whose turn-on energy is relatively large but the turn-off energy is negligible.

In [10-12], high-frequency CRM control is proposed to achieve soft switching and good power factor for a single-phase bi-directional AC/DC converter. With inductor current zero-crossing-detection (ZCD) and programmed off-time extension, whole-line ZVS soft switching is achieved to reduce switching loss and improve efficiency. With average current mode control, good power factor and low total-harmonic-distortion (THD) are achieved. Experiment results show that with this high-frequency CRM control, 98.5% peak efficiency is achieved for bi-directional operation with switching frequency above 300 kHz.

Therefore, in single-phase AC/DC converters, CRM soft switching is beneficial for high switching frequency operation. Then the question is whether CRM soft switching can be implemented in three-phase AC/DC converters with good performance at high switching frequency operation as well.

However, in three-phase AC/DC converters, since the summation of currents in all three phases are always equal to zero, only two phases among all the three phases are independent. Therefore, independent CRM control cannot be

achieved for all three phases at the same time, which is the main challenge of the CRM control in three-phase AC/DC converters. In order to overcome this challenge, two methods are proposed and reported in literature [13-14]. In these two methods, split capacitors are used at DC side and the middle point is connected to the AC side neutral point to decouple three phases. Although by this means each phase can be controlled as CRM independently, in high switching frequency and high modulation index (the ratio of AC line-to-line peak voltage to DC voltage) design, switching frequency variation range over line cycle is extremely wide (from 300 kHz to >6 MHz) when using either of these two methods. Although time-variant switching frequency is an intrinsic feature for CRM operation, too wide switching frequency variation range causes high switching related loss.

Thus, CRM-based soft switching modulation for three-phase bi-directional AC/DC converters is proposed and applied in inverter mode applications in [15]. By adopting discontinuous-pulse-width-modulation (DPWM) as a means of decoupling, and discontinuous conduction mode (DCM) for switching frequency synchronization to limit switching frequency range, 98.9% peak efficiency is achieved with switching frequency above 300 kHz under inverter mode operation.

This paper is focused on the implementation of the proposed modulation into rectifier mode applications. The two improvements of the implementation in rectifier mode operation are: (1) programmed off-time extension to solve the non-ZVS issue and (2) using negative coupled inductors to ensure stable operation. In this paper, first, bi-directional three-phase CRM-based soft-switching modulation in [15] is briefly reviewed in Section II. Then, the non-ZVS issue for rectifier mode is discussed and the solution is provided in Section III. After that, the use of negative coupled inductors is discussed in Section IV. Finally, hardware implementation and experiment results of the proposed modulation in rectifier mode operation are shown in Section V.

II. Review of Three-Phase Soft-Switching Modulation for Inverter/Rectifier

Although decoupling among three phases can be achieved by the connection between the DC side middle point and the AC side neutral point, it causes wide switching frequency range. Therefore, alternative method of decoupling among three phases is necessary.

Therefore in [15], the discontinuous pulse width modulation (DPWM) is adopted as the method of decoupling, enabling the other two phases to be independently controlled as CRM operation. To minimize switching loss, the DPWM clamping option is determined by the peak and polarity of AC reference current.

As for the circuit topology, two-level H-bridge structure shown in Fig. 1 is selected for analysis since this is the simplest topology for three-phase bi-directional AC/DC converters.

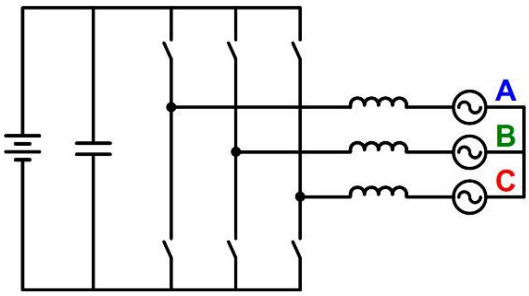

Fig. 1. Three-phase H-bridge structure.

However, with one phase clamped and the other two phases controlled at CRM independently (Refer to [15] for detailed control diagram), although the switching frequency variation range is improved to some degree compared with using the two methods reported in literature, the variation range is still wide. With minimum switching frequency at 300 kHz, the peak switching frequency is around 3 MHz. The switching frequency distribution in half line cycle is shown in Fig. 2. This wide switching frequency variation range still causes large switching related loss, which is unacceptable.

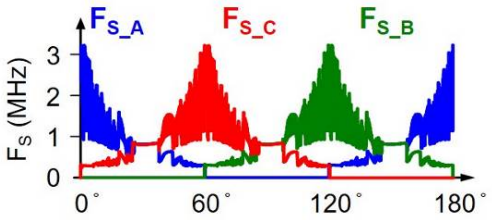

Fig. 2. Three-phase switching frequency distribution in half line cycle with DPWM-based CRM modulation (The blue/green/red curve is the switching frequency distribution in phase A/B/C respectively).

From Fig. 2, except for the phase operating at clamping mode, one phase operates at relatively higher switching frequency, while the other phase operates at relatively lower switching frequency. Take the first 30-degree time interval in the half line cycle as an example. The switching frequency in phase A is higher than that in phase C. In order to limit the switching frequency in phase A, the operation mode in phase A is changed from CRM to discontinuous conduction mode (DCM). The turn-on instant in phase A is synchronized to that in phase C and thus the switching frequency in phase A is synchronized to phase C, which means the turn-on of both phase A and C are determined by the inductor current zero crossing of phase C. Taking the inverter mode operation as an example, the waveforms of gate signals of control switches and inductor currents in phase A and C are shown in Fig. 3(a). Apply above analysis to the whole line cycle, and the operation mode distribution with above modulation (called "DPWM + CRM + F_S sync" for short) in line cycle is shown in Fig. 3(b).

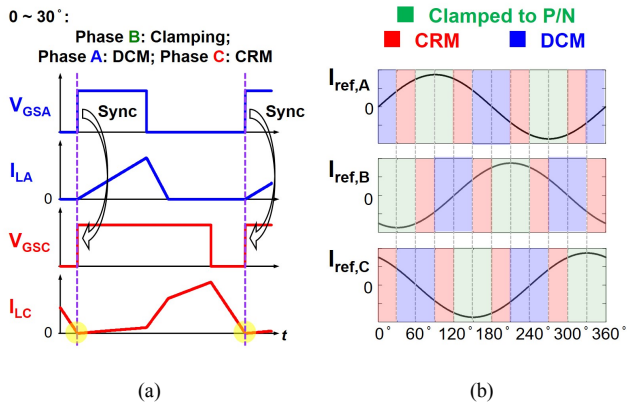

Fig. 3. After switching frequency synchronization: (a) Switching-cycle waveforms ($V_{GSA/C}$: gate signal of the control switch in phase A/C respectively; $I_{LA/C}$: inductor current in phase A/C respectively) (b) Line-cycle operation mode distribution ($I_{ref,A/B/C}$: AC reference current in phase A/B/C respectively; Example: for the first 30-degree time interval, phase A/B/C operate at DCM/CRM/clamping mode respectively).

As shown in Fig. 4, keeping the minimum switching frequency the same as 300 kHz, the switching frequency range after frequency synchronization (in multicolor) is significantly reduced (only from 300 kHz to 500 kHz) compared with the frequency range before frequency synchronization (in gray), thus reducing switching related loss. Based on this modulation, simulation in [15] shows that total device related loss is 0.5% of total power, and the peak efficiency is projected to be around 99%.

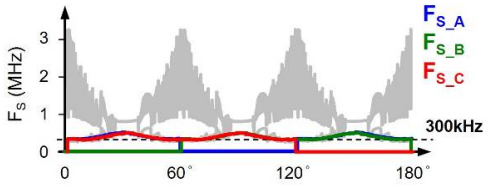

Fig. 4. Comparison of switching frequency distributions before and after switching frequency synchronization (Gray: switching frequency range before frequency synchronization; Blue/Green/Red: switching frequency range after frequency synchronization).

This "DPWM + CRM + F_S sync" modulation is applicable to both inverter mode and rectifier mode operations. It is discussed in detail for PV inverter application, and the basic control functions have been experimentally verified in [15]. This paper focuses on the implementation of this modulation into rectifier mode applications. The two improvements of the implementation in rectifier mode operation will be discussed below. The first one is programmed off-time extension to solve the non-ZVS issue, and the second one is using negative coupled inductors to ensure stable operation.

III. Off-Time Extension For Zero-Voltage-Switching (ZVS) in Rectifier Mode

ZVS turn-on is an important aspect of the good performance with the "DPWM + CRM + F_S sync" modulation. Take the first 30-degree interval as an example, when phase A and C are operating at DCM and CRM, respectively. The negative current due to LC resonance (L: inductor; C: junction capacitor, C_{oss} of devices) after inductor current zero crossing is beneficial for achieving ZVS. With this modulation, the simulation results in [15] have shown that under inverter mode operation at typical condition (V_{DC} = 800 V, $V_{AC\ (L\text{-}L,\ RMS)}$ = 480 V), ZVS is achieved naturally during CRM operation, and although ZVS is not necessarily achieved during DCM operation, valley switching can be achieved by slight turn-on delay during DCM operation to minimize DCM turn-on loss.

However, in rectifier mode, under the same operating condition, ZVS turn-on cannot be achieved naturally during CRM operation. Simulation in Fig. 5(a) shows switching-cycle waveforms, including gate signal, inductor current and drain-source voltage of control switch, at arbitrarily selected two instants during CRM operation. At each instant, drain-source voltage cannot reach zero during LC resonance, which indicates that ZVS cannot be achieved naturally in rectifier mode.

Insufficient negative current is the reason for non-ZVS in rectifier mode. To provide more negative current, after inductor current zero crossing happens, off-time is extended by making the synchronous rectifier (SR) conduct for an extra period of time [10, 16-19]. Fig. 5(b) shows switching cycle waveforms with off-time extension (highlighted in yellow color) at the same instant as in Fig. 5(a). From Fig. 5(b), at each instant, drain-source voltage reaches zero during LC resonance, which means ZVS is achieved. Thus, off-time extension is required in rectifier mode operation for ZVS.

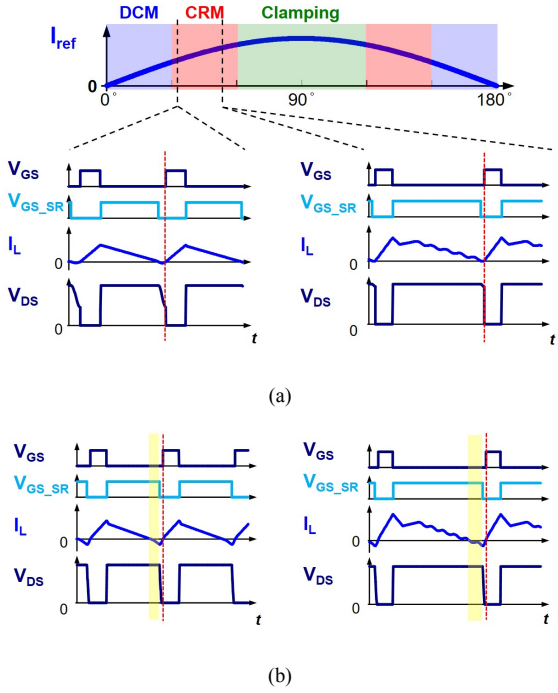

Fig. 5. Switching-cycle waveforms in rectifier mode during CRM (a) without extension (non-ZVS) (b) with extension (ZVS) (I_{ref}: AC reference current; for all the switching-cycle waveforms, V_{GS}: gate signal of the control switch; V_{GS_SR}: gate signal of the synchronous rectifier, SR; I_L: inductor current; V_{DS}: drain-source voltage of the control switch).

Then the remaining issue is how to determine the required period of time for off-time extension (the period of time highlighted in yellow color in Fig. 5(b)). Since phase A operates at DCM and phase C operates at CRM, after the inductor current zero crossing happens in phase C, both phase A and C are participating the LC resonance, and the equivalent circuit becomes a 4th-order LC circuit, which is hard to find analytical solutions compared with the equivalent 2nd-order LC circuit in single-phase AC/DC converters [10].

Therefore, simulation is used as a numerical method to derive the required period of time for off-time extension. From simulation results, under the typical operating condition (V_{DC} = 800 V, $V_{AC\ (L\text{-}L,\ RMS)}$ = 480 V), during the first 30-degree interval, the required negative current at 0-degree instant is -9A, and the required negative current at 30-degree instant is -7A. The required negative current between 0 and 30-degree instants can be determined by linear interpolation. Based on these required negative current values and the inductor current slew rate during the period of off-time extension, the required period of time for off-time extension can be then determined.

As for ZVS turn-on during DCM operation, similar to the inverter mode operation, slight turn-on delay is also required to achieve valley switching turn-on. Still taking the first 30-degree interval as an example. In Fig. 6, the drain-source voltage in phase C reaches zero at the beginning of the green shaded interval. And then, the control switch in phase A is not turned on until when the drain-source voltage in phase A reaches valley point (the end of the green shaded interval). It can be seen that with the turn-on delay in phase A (green shaded interval), phase A's drain-source voltage is also discharged to valley point, which minimizes DCM turn-on loss. The turn-on delay can be determined by the LC resonance period in the equivalent 2nd-order LC circuit during green shaded interval.

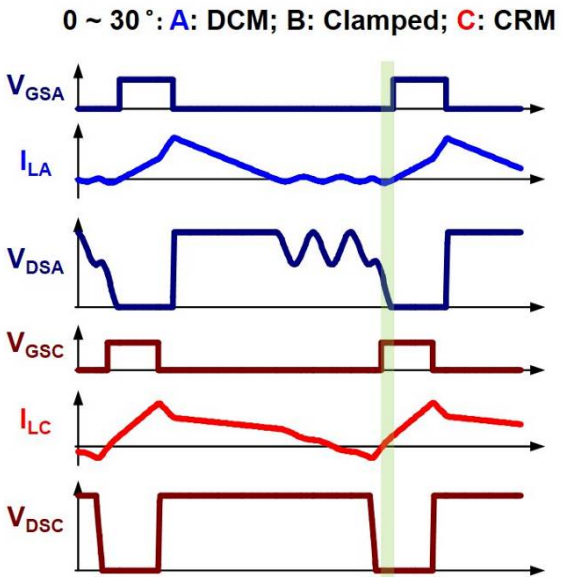

Fig. 6. Switching-cycle waveforms in phase A and phase C during the first 30-degree time interval ($V_{GSA/C}$: gate signal of the control switch in phase A/C; $I_{LA/C}$: inductor current in phase A/C; $V_{DSA/C}$: drain-source voltage of the control switch in phase A/C).

IV. Two-Channel Interleaved Rectifier with Negative Coupled Inductors

For higher power application, one or more channels (phase legs) can be added into each phase. Here Fig. 7 shows the circuit diagram of three-phase H-bridge structure, with two channels in each phase as an example. What's more, multi-channel interleaving control is widely used for current ripple cancellation to overcome the drawback of large current ripple in CRM operation, which is beneficial for harmonic and EMI filter size reduction [20-24]. Here, two-channel interleaving is applied, which means the two channels in each phase operate with 180-degree phase-shift in each switching cycle. The open-loop interleaving control method [20-21], which is more suitable for the digital controlled system with high switching frequency operation [24], is applied here for the implementation of the two-channel interleaving control.

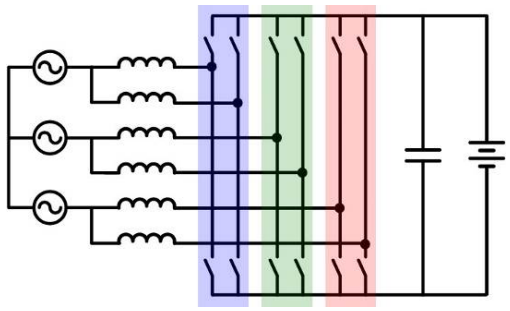

Fig. 7. Circuit of three-phase AC/DC converter with two legs in each phase.

The control goal of two-channel interleaving is to make the phase-shift between two channels exactly 180 degrees. In open-loop interleaving control method, for the two channels in each phase, one is defined as master, and the other one as slave. For the master channel, the turn-on instant is determined by inductor current zero crossing, and the turn-off instant is determined by average current loop. According to the real-time measurement of the switching period in master channel, for the slave channel, the turn-on and the turn-off instants are always delayed by 180 degrees (one half of the measured switching period in previous switching cycle) compared with master channel.

Since here the switching frequency is time-variant during whole line cycle, change of switching period in master channel will cause phase error and impact the switching actions in slave channel, because it always needs some time for interleaving control to be executed. Also switching actions in one channel will impact voltage excitation across inductor in the other channel through AC side common node. The switching action in slave channel will also impact the inductor volt-second, and thus the switching period in master channel. Therefore, a new feedback loop related to interleaving is formed with the proposed modulation. Instability issue exists when the phase margin of this feedback loop is insufficient.

Fig. 8 shows the line-cycle and switching-cycle waveforms in two-channel interleaved rectifier mode operation, including the master-channel individual inductor current and the total inductor current in phase A. It can be seen that instability exists in two-channel interleaved rectifier mode operation. In two-

channel interleaved inverter mode operation, the instability issue does not exist (Refer to [15] for detailed results).

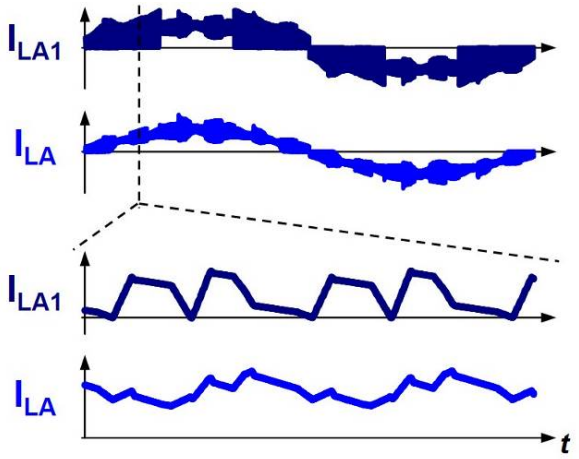

Fig. 8. Line-cycle and switching-cycle inductor current waveforms in two-channel interleaved rectifier mode (I_{LA1} is the master-channel individual inductor current in phase A; I_{LA} is the total inductor current in phase A).

The main reason of the instability in two-channel-interleaved rectifier mode is that the current ramp before master channel inductor current (I_{LA1}) zero crossing point is very small, while this current ramp in inverter mode is large. The small current ramp will make the small signal modulation gain and bandwidth of the aforementioned feedback loop high, and thus phase margin is insufficient to maintain stable operation when there is perturbation (time-variant switching frequency/period in whole line cycle).

The instability issue in two-channel-interleaved rectifier mode can be solved by using negative coupled inductor, which means that in each phase, the two individual inductors in each channel is inversely coupled with each other. The circuit diagram with negative coupled inductor is shown in Fig. 9.

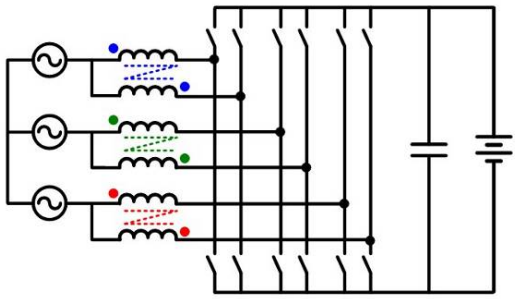

Fig. 9. Three-phase AC/DC converter with negative coupled inductors.

Fig. 10 shows the line-cycle and switching-cycle waveforms in two-channel interleaved rectifier mode operation with negative coupled inductors, including the master-channel individual inductor current and the total inductor current in phase A. Negative coupling increases the current ramp by changing equivalent inductance before master channel inductor current zero crossing point, which can be clearly seen from Fig. 10 when compared with Fig. 8. Larger current ramp makes small signal modulation gain become lower, and thus provides sufficient phase margin to maintain stability, which is clearly shown in Fig. 10.

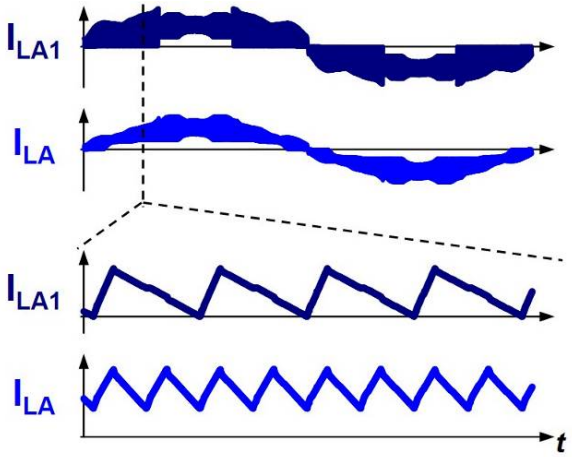

Fig. 10. Line-cycle and switching-cycle inductor current waveforms in two-channel interleaved rectifier mode with negative coupled inductors (I_{LA1} is the master-channel individual inductor current in phase A; I_{LA} is the total inductor current in phase A).

It should also be noted that the negative coupling effect should be strong enough to totally eliminate the instability (sub-harmonic oscillation). From simulation, the boundary of coupling coefficient is about -0.45 under the typical operating condition (V_{DC} = 800 V, $V_{AC\ (L\text{-}L,\ RMS)}$ = 480 V). The negative coupling coefficient boundary is related to the modulation index (the ratio of AC line-to-line peak voltage to DC voltage). Lower modulation index results in smaller absolute value of negative coupling coefficient boundary. The theoretical derivation of the negative coupling coefficient boundary will be included in future publication.

V. Experiment Results

According to the system diagram in Fig. 9, a 25 kW bi-directional three-phase AC/DC converter prototype is built with 1.2 kV 25mΩ SiC MOSFETs, which is shown in Fig. 11. The SiC MOSFETs used in this prototype are from GE with DE-150 package, which is very suitable for hundreds of kHz high frequency application due to the good decoupling between the driving loop and the power loop. (Refer to [10] for detailed device parameters) The power density of this prototype is 80W/in^3, including all voltage and current sensors, DC-link capacitors, LC harmonic filters, and the space reserved for heat sinks. The inductance value for the converter-side inductors is designed to make the minimum switching frequency over a line cycle equal to 300 kHz. For non-interleaved operation, the required inductance value is 3.5μH. And for two-channel-interleaved operation, since negative coupled inductors are required and the negative coupling effect should be strong enough, the coupling coefficient value is selected as -0.6 and then the self-inductance value is selected as 6μH. The control is implemented digitally with one microcontroller (MCU), TMS320F28075, from TI, and the control cycle, or the interrupt service routine (ISR) period is 3μs.

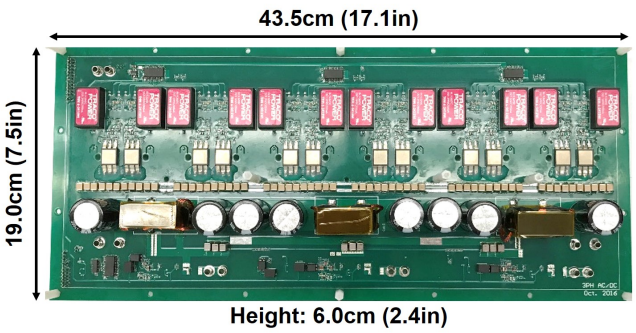

Fig. 11. Prototype of 25 kW SiC-based bi-directional three-phase AC/DC converter.

Using the prototype shown in Fig. 11, the experimental verifications of the implementation of all the control functions and the capability of power density under inverter mode operation have been illustrated in [15]. Under non-interleaved inverter mode operation, the tested peak efficiency is 98.9%. Under two-channel-interleaved inverter mode operation, the tested peak efficiency is 99.0%. The slight improvement of efficiency is due to the reduction of individual inductor current ripple and thus the reduction of conduction loss and inductor loss in the two-channel-interleaved operation.

The same hardware prototype in Fig. 11 is used for rectifier mode experimental verifications. For non-interleaved rectifier mode operation (only one channel per phase is working and the full power is 12.5 kW), Fig. 12 shows the typical line-cycle experiment waveforms, including the waveforms of AC line-to-line voltage, gate signal and drain-source voltage of the bottom switch, and the inductor current.

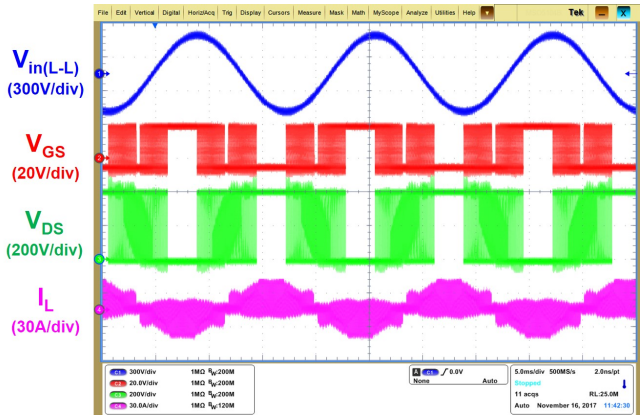

Fig. 12. Line-cycle experiment waveforms under non-interleaved rectifier mode operation (CH1 is the input AC line-to-line voltage; CH2 is the V_{GS} of the bottom switch in phase A; CH3 is the V_{DS} of the bottom switch in phase A; CH4 is the inductor current in phase A).

Two instants are arbitrarily selected during the time interval with CRM operation, and the typical switching-cycle experiment waveforms are shown in Fig. 13. It can be seen that at each instant, before the bottom switch is turned on, its drain-source voltage has already reached zero, which verifies that ZVS is achieved at any instant during CRM operation.

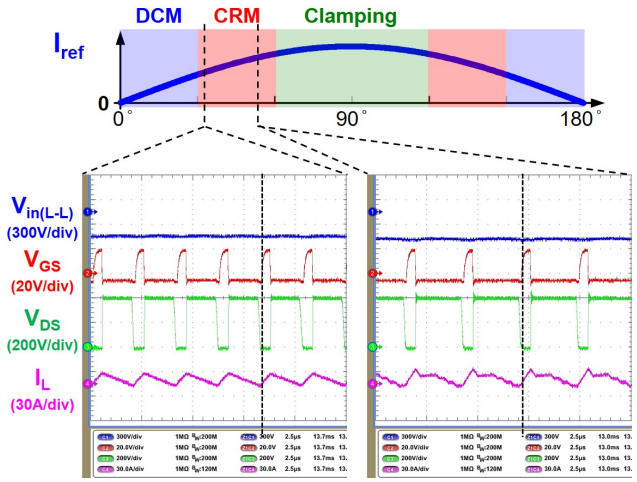

Fig. 13. Switching-cycle experiment waveforms during CRM mode under non-interleaved rectifier mode operation (CH1 is the input AC line-to-line voltage; CH2 is the V_{GS} of the bottom switch in phase A; CH3 is the V_{DS} of the bottom switch in phase A; CH4 is the inductor current in phase A).

Similarly, two instants are arbitrarily selected during the time interval with DCM operation, and the typical switching-cycle experiment waveforms are shown in Fig. 14. It can be seen that at each instant, before the bottom switch is turned on, its drain-source voltage has already reached valley point, which verifies that valley switching is achieved at any instant during DCM operation and the DCM turn-on loss is minimized.

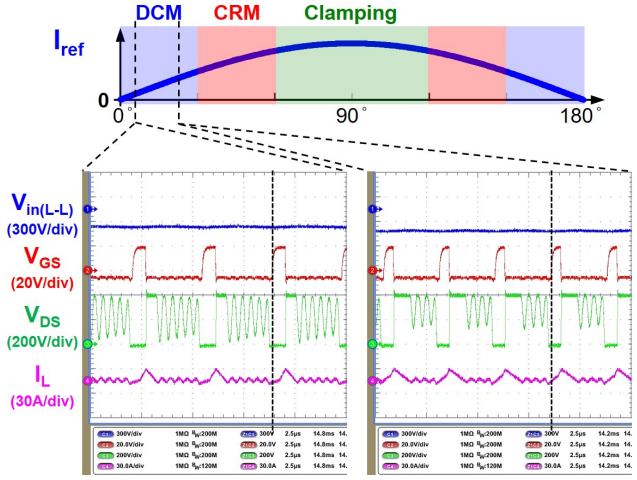

Fig. 14. Switching-cycle experiment waveforms during DCM mode under non-interleaved rectifier mode operation (CH1 is the input AC line-to-line voltage; CH2 is the V_{GS} of the bottom switch in phase A; CH3 is the V_{DS} of the bottom switch in phase A; CH4 is the inductor current in phase A).

The same hardware prototype is used in inverter mode and rectifier mode test, and the modulation under these two operations is similar. Both inverter mode and rectifier mode operations can achieve ZVS soft switching with similar switching frequency range, so it can be expected that the peak efficiency for rectifier mode operation is similar to that in inverter mode operation. The simulated efficiency at rated voltage under different power levels for rectifier mode

operation is shown in Fig. 15, together with the efficiency test results for inverter mode operation at rated conditions. Also, the preliminary efficiency test result at $240V_{AC\ (L\text{-}L,\ RMS)}$, $400V_{DC}$ and 3kW condition is 99.0%. The efficiency test under higher voltage and power conditions for rectifier mode operation is still in progress. The testing results will be included in future publication.

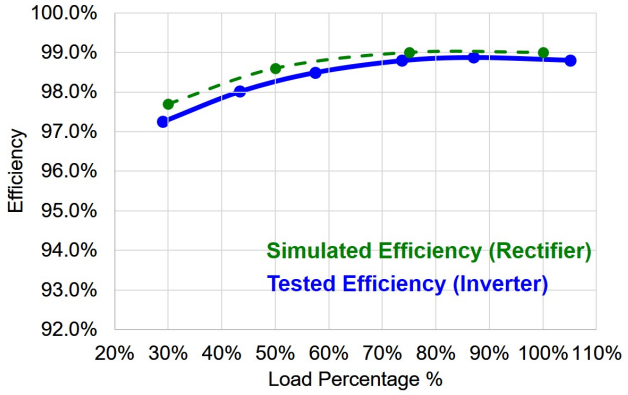

Fig. 15. Comparison between simulated efficiency in rectifier mode operation and test efficiency in inverter mode operation.

VI. CONCLUSIONS

A novel CRM-based soft-switching modulation (DPWM + CRM + F_S sync) is proposed for three-phase bi-directional AC/DC converters, which is able to achieve ZVS soft switching turn-on and limit switching frequency variation range to improve efficiency especially at hundreds of kHz high switching frequency operations. Based on the detailed analysis in inverter mode operation in [15], this modulation is applied into rectifier mode application in this paper. Different from inverter mode operation, two issues exist in rectifier mode operation and corresponding solutions are provided. Off-time extension is required for achieving ZVS during CRM operation. Negative coupled inductors are required to maintain stable operation in two-channel-interleaved rectifier mode operation. Simulation results verify the above solutions, and all the control functions are implemented digitally using microcontroller on a 25 kW three-phase bi-directional AC/DC converter prototype with 80 W/in^3 power density. For both inverter mode and rectifier mode operation, the peak efficiency is 99.0% at above 300 kHz switching frequency operation.

REFERENCES

[1] "Supercharger," http://www.teslamotors.wiki/wiki/Supercharger.

[2] US 8810208 B2, "Charging efficiency using selectable isolation," US patent, Mar. 2011.

[3] D. Aggeler et al., "Ultra-fast DC-charge infrastructures for EV-mobility and future smart grids," 2010 IEEE PES Innovative Smart Grid Technologies Conference Europe (ISGT Europe), Gothenburg, 2010, pp. 1-8.

[4] B. Guo, "High-Efficiency Three-Phase Current Source Rectifier Using SiC Devices and Delta-Type Topology," Ph.D. Dissertation, The University of Tennessee, Knoxville, 2014.R. Nicole, "Title of paper with only first word capitalized," J. Name Stand. Abbrev., in press.

[5] Electric Vehicle Charging Infrastructure, ABB, http://new.abb.com/ev-charging/multi-standard/terra-53-cj-ul

[6] M. Mu and F. C. Lee, "Comparison and optimization of high frequency inductors for critical model GaN converter operating at 1MHz," *2014 International Power Electronics and Application Conference and Exposition*, Shanghai, 2014, pp. 1363-1368.

[7] Y. Yang, M. Mu, Z. Liu, F. C. Lee and Q. Li, "Common mode EMI reduction technique for interleaved MHz critical mode PFC converter with coupled inductor," *2015 IEEE Energy Conversion Congress and Exposition (ECCE)*, Montreal, QC, 2015, pp. 233-239.

[8] C. DiMarino, Z. Chen, M. Danilovic, D. Boroyevich, R. Burgos and P. Mattavelli, "High-temperature characterization and comparison of 1.2 kV SiC power MOSFETs," *2013 IEEE Energy Conversion Congress and Exposition*, Denver, CO, 2013, pp. 3235-3242.

[9] C. DiMarino, Z. Chen, D. Boroyevich, R. Burgos and P. Mattavelli, "Characterization and comparison of 1.2 kV SiC power semiconductor devices," *2013 15th European Conference on Power Electronics and Applications (EPE)*, Lille, 2013, pp. 1-10.

[10] Z. Liu, B. Li, F. C. Lee and Q. Li, "High-Efficiency High-Density Critical Mode Rectifier/Inverter for WBG-Device-Based On-Board Charger," in *IEEE Transactions on Industrial Electronics*, vol. 64, no. 11, pp. 9114-9123, Nov. 2017.

[11] Y. Yang, Z. Liu, F. C. Lee and Q. Li, "Multi-phase coupled and integrated inductors for critical conduction mode totem-pole PFC converter," *2017 IEEE Applied Power Electronics Conference and Exposition (APEC)*, Tampa, FL, 2017, pp. 1804-1809.

[12] B. Li, F. C. Lee, Q. Li and Z. Liu, "Bi-directional on-board charger architecture and control for achieving ultra-high efficiency with wide battery voltage range," *2017 IEEE Applied Power Electronics Conference and Exposition (APEC)*, Tampa, FL, 2017, pp. 3688-3694.

[13] D. Zhang, Q. Zhang, H. Hu, A. Grishina, J. Shen and I. Batarseh, "High efficiency current mode control for three-phase micro-inverters," *2012 Twenty-Seventh Annual IEEE Applied Power Electronics Conference and Exposition (APEC)*, Orlando, FL, 2012, pp. 892-897.

[14] D. Leuenberger, D. Christen, and J. Biela, "Triangular Current Mode Operation of a Three Phase Interleaved T-Type Inverter for Photovoltaic Systems," in *Proc. PCIM Europe*, 8- 10 May, Nuremberg, 2012.

[15] Z. Huang, Z. Liu, F. C. Lee, Q. Li and F. Xiao, "Critical-mode-based soft-switching modulation for three-phase inverters," *2017 IEEE Energy Conversion Congress and Exposition (ECCE)*, Cincinnati, OH, USA, 2017, pp. 167-174.

[16] B. Su, J. Zhang and Z. Lu, "Totem-Pole Boost Bridgeless PFC Rectifier With Simple Zero-Current Detection and Full-Range ZVS Operating at the Boundary of DCM/CCM," in *IEEE Transactions on Power Electronics*, vol. 26, no. 2, pp. 427-435, Feb. 2011.

[17] Z. Liu, F. C. Lee, Q. Li and Y. Yang, "Design of GaN-Based MHz Totem-Pole PFC Rectifier," in *IEEE Journal of Emerging and Selected Topics in Power Electronics*, vol. 4, no. 3, pp. 799-807, Sept. 2016.

[18] Z. Liu, Z. Huang, F. C. Lee, Q. Li and Y. Yang, "Operation analysis of digital control based MHz totem-pole PFC with GaN device," *2015 IEEE 3rd Workshop on Wide Bandgap Power Devices and Applications (WiPDA)*, Blacksburg, VA, 2015, pp. 281-286.

[19] Z. Huang, Z. Liu, Q. Li and F. C. Lee, "Microcontroller-based MHz totem-pole PFC with critical mode control," *2016 IEEE Energy Conversion Congress and Exposition (ECCE)*, Milwaukee, WI, 2016, pp. 1-8.

[20] T. Ishii and Y. Mizutani, "Power factor correction using interleaving technique for critical mode switching converters," *PESC 98 Record. 29th Annual IEEE Power Electronics Specialists Conference (Cat. No.98CH36196)*, Fukuoka, 1998, pp. 905-910 vol.1.

[21] L. Huber, B. T. Irving and M. M. Jovanovic, "Open-Loop Control Methods for Interleaved DCM/CCM Boundary Boost PFC Converters," in *IEEE Transactions on Power Electronics*, vol. 23, no. 4, pp. 1649-1657, July 2008.

[22] M. S. Elmore, "Input current ripple cancellation in synchronized, parallel connected critically continuous boost converters," *Applied Power Electronics Conference and Exposition, 1996. APEC '96.*

Conference Proceedings 1996., Eleventh Annual, San Jose, CA, 1996, pp. 152-158 vol.1.

[23] L. Huber, B. T. Irving and M. M. Jovanovic, "Review and Stability Analysis of PLL-Based Interleaving Control of DCM/CCM Boundary Boost PFC Converters," in *IEEE Transactions on Power Electronics*, vol. 24, no. 8, pp. 1992-1999, Aug. 2009.

[24] Z. Liu, Z. Huang, F. C. Lee and Q. Li, "Digital-Based Interleaving Control for GaN-Based MHz CRM Totem-Pole PFC," in *IEEE Journal of Emerging and Selected Topics in Power Electronics*, vol. 4, no. 3, pp. 808-814, Sept. 2016.